Differential immune microenvironments and response to immune checkpoint blockade amongst molecular subtypes of murine medulloblastoma

Christina D. Pham[1,2], **Catherine Flores**[1], **Changlin Yang**[1], **Elaine M. Pinheiro**[4], **Jennifer H. Yearley**[4], **Elias J. Sayour**[1,2], **Yanxin Pei**[5], **Colin Moore**[6], **Roger E. McLendon**[2], **Jianping Huang**[1], **John H. Sampson**[2,3], **Robert Wechsler-Reya**[6], and **Duane A. Mitchell**[1,†]

[1]Preston A. Wells, Jr. Center for Brain Tumor Therapy, UF Brain Tumor Immunotherapy Program, Department of Neurosurgery, McKnight Brain Institute, University of Florida, Gainesville, FL

[2]Department of Pathology, Duke University Medical Center, Durham, NC

[3]Department of Neurosurgery, Duke University Medical Center, Durham, NC

[4]Merck & Co., Inc., Kenilworth, New Jersey

[5]Cancer and Immunology Department, Brain Tumor Institute, Children's National Medical Center, Washington DC

[6]Tumor Initiation and Maintenance Program, Sanford-Burnham Medical Research Institute, La Jolla, CA

Abstract

PURPOSE—Despite significant strides in the identification and characterization of potential therapeutic targets for medulloblastoma (MB), the role of the immune system and its interplay with the tumor microenvironment within these tumors are poorly understood. To address this, we adapted two syngeneic animal models of human Sonic Hedgehog (SHH)-driven and Group 3 MB for preclinical evaluation in immunocompetent C57BL/6 mice.

METHODS AND RESULTS—Multicolor flow cytometric analyses were used to phenotype and characterize immune infiltrating cells within established cerebellar tumors. We observed significantly higher percentages of dendritic cells, infiltrating lymphocytes, myeloid derived suppressor cells and tumor-associated macrophages in murine SHH model tumors compared with Group 3 tumors. However, murine Group 3 tumors had higher percentages of CD8$^+$ PD-1$^+$ T cells

†**Corresponding author:** Duane A. Mitchell; Preston A. Wells, Jr. Center for Brain Tumor Therapy, UF Brain Tumor Immunotherapy Program, Department of Neurosurgery, UF Medical Center; 1149 S Newell Dr, L2-100, Gainesville, FL 32611; duane.mitchell@neurosurgery.ufl.edu.

within the CD3 population. PD-1 blockade conferred superior antitumor efficacy in animals bearing intracranial Group 3 tumors compared to SHH group tumors, indicating that immunologic differences within the tumor microenvironment can be leveraged as potential targets to mediate antitumor efficacy. Further analysis of anti-PD-1 monoclonal antibody localization revealed binding to PD-1+ peripheral T cells, but not tumor infiltrating lymphocytes within the brain tumor microenvironment. Peripheral PD-1 blockade additionally resulted in a marked increase in CD3+ T cells within the tumor microenvironment.

CONCLUSIONS—This is the first immunologic characterization of preclinical models of molecular subtypes of MB and demonstration that response to immune checkpoint blockade differs across subtype classification. Our findings also suggest that effective anti-PD-1 blockade does not require that systemically administered antibodies penetrate the brain tumor microenvironment.

INTRODUCTION

Medulloblastoma (MB), the most common malignant primary brain tumor of childhood, remains incurable in approximately one-third of patients despite surgical resection, radiation therapy and aggressive chemotherapy (1⁻3). Patients endure significant morbidities from such treatments, thus necessitating more targeted strategies that utilize accurate molecular subtype classification (1⁻3). Mediating consistent and safe treatment for MB patients represents the next goal in achieving an unmet need for the successful eradication of these malignancies (4).

Immunotherapy presents an effective approach that has shown considerable advances in generating sustained and robust antitumor responses in malignant gliomas (5). However, the exploration of immune based strategies in pediatric brain tumors has been limited and to date, with few successful applications reported for MB patients (6, 7). A considerable obstacle in the development of MB immunotherapy has been a lack of understanding regarding the complex immunologic interactions that occur within the tumor microenvironment. Recent immunohistochemistry (IHC) and gene expression evidence has shed some light on the immunologic phenotype across MB subtypes and shown that tumor-associated macrophage and inflammatory gene upregulation could additionally be used to stratify the different molecular subgroups (8). These observations demonstrate that MB tumor subtypes contain highly distinct immune profiles, and further suggest that each subgroup may have different mechanisms of facilitating immune suppression and evasion. Despite a plethora of genetic and histopathological information from patient samples, an absence of relevant preclinical animal models has also hindered the investigation of promising immunotherapeutic targeting strategies of MB *in vivo*.

Here, we demonstrate the successful adaptation and immune characterization of two intracranial syngeneic animal models recapitulating human Sonic Hedgehog (SHH) and Group 3 MB. The SHH MB group tumors recapitulate the phenotype of pathologically classified 'classic' and 'desmoplastic' human MBs, while the Group 3 MB group tumors comprise the more invasive and aggressive 'anaplastic' human MBs (9). Among the first genetically engineered models of SHH-driven MB, the *Patched* homolog 1 (*Ptch1*)-knock

out mouse was generated through homologous recombination of the *Ptch1* gene, causing a loss of PTCH1 protein expression and constitutive SHH pathway activation (10). While homozygous mutations in the *Ptch1* gene are embryonically lethal, heterozygotes (*Ptch1*$^{+/-}$) are viable and form MB tumors in 15-20% of mice at 16-25 weeks (10⁻12). In addition to the Ptch1 model of SHH-associated MB (Ptch 1 MB), a model of MYC-amplified MB or human Group 3 MB (hereafter referred to as neural stem cell MB or NSC MB) was originally created through the retroviral transduction of sorted cerebellar granule neuron precursor cells (CD133$^+$, lineage negative cells from the postnatal day 5 cerebellum) with genes encoding a stable form of *Myc* and a dominant negative form of *p53* (13). Infected cells were implanted into the cerebella of immune deficient NOD scid IL-2 receptor gamma knockout (NSG) mice and formed tumors within 6-12 weeks (13). We adapted the aforementioned models for immunotherapeutic assessment through orthotopic transplantation of each tumor type into the cerebella of immune competent C57BL/6 hosts. After several passages, we produced a large stock of Ptch1 MB and NSC MB tumor cells that could be stereotactically implanted to generate large cohorts of uniformly tumor-bearing animals.

After successful adaptation and validation of these models, we characterized the tumor infiltrating immune cells in both animal models of MB. We analyzed both myeloid and T cell populations and further investigated markers of activated and suppressive immune cell phenotypes. Ptch1 MB tumors contained significantly increased frequencies of infiltrating dendritic cells, T cells and myeloid cells in comparison to NSC MB tumors. However, higher percentages CD8$^+$ PD-1$^+$ T cells of infiltrating CD3$^+$ cells were identified in NSC MB tumors. We show that *in vivo* blockade of the PD-1 expressing lymphocyte population showed a significant antitumor benefit in intracranial NSC MB-bearing animals, but not in Ptch1 MB animals. Further analysis of treated tumors in both subtypes revealed anti-PD-1 monoclonal antibody to be only bound to PD-1+ T cells in peripheral lymphoid organs and absent on tumor infiltrating lymphocytes in the brain. PD-1 blockade also resulted in significant increases in infiltrating PD-1 negative T cells within the tumor microenvironment. Our findings suggest that MB subgroups have distinct immune profiles that may require different immunotherapeutic targeting strategies to mediate antitumor immunity.

MATERIALS AND METHODS

Tumor Cells

Ptch+/− mutant mice and NSC MB (MP) cells were provided in collaboration with Dr. Robert Wechsler-Reya (Sanford-Burnham Research Institute, La Jolla, CA). The NSC MB tumor was originally isolated from a tumor arising from implanted cerebellar stem cells that had been retrovirally transduced with mutations in *p53* and *c-myc* (13). The Ptch1 MB tumor was isolated from a spontaneously arising tumor in the Ptch1$^{+/-}$ mutant mouse on a C57BL/6 background (10). Both tumors were passaged *in vivo* six times in the C57BL/6 background. Explanted tumor cells from the sixth passage were frozen down and used for all subsequent optimization and efficacy experiments.

Mice

Five to eight week old C57BL/6 mice were obtained from the Jackson Laboratory (Bar Harbor, ME). The investigators adhered to the "Guide for the Care and Use of Laboratory Animals" as proposed by the committee on Care of Laboratory Animal Resources Commission on Life Sciences, National Research Council. The facilities at the Duke Cancer Center Isolation Facility and the University of Florida Biomedical Science Building are fully accredited by the American Association for Accreditation of Laboratory Animal Care, and all studies were approved by the Duke University and University of Florida Institutional Animal Care and Use Committee.

Intracranial tumor implantation

Frozen tumor cells were thawed and immediately washed twice with sterile PBS. For intracerebellar NSC MB tumor implantation, cells were mixed 50/50 with 10% methylcellulose in PBS and loaded into a 250 μL syringe (Hamilton) with an attached 25-gauge needle. For intracerebellar Ptch1 MB tumor implantation, cells were mixed in PBS and loaded into a 5 μL syringe (Hamilton). Mice were positioned into a Kopf stereotactic frame and a ½ inch incision was made at the midline of the scalp over the position of the cerebellum. Implantation into the cerebellum was measured at 1 mm lateral to the midline at a depth of 3mm. Based on tumorgenicity studies, a minimum tumorigenic dose of 1×10^3 NSC MB cells and 1.25×10^5 Ptch1 MB cells were implanted in subsequent survival studies.

Microarray Analyses

RNA was isolated from tumor cells using the RNeasy Mini Kit (Qiagen). RNA was labeled and hybridized to Affymetrix Mouse Genome 430 2.0 arrays. Microarray data were processed using robust multichip analysis (RMA) in Partek Genomics Suite 6.5 (Partek, Inc.). Differentially expressed genes were identified by using ANOVA. Genes were selected based on a fold change cut off >2 and P-value with FDR < 0.05.

Immunohistochemistry

Tissue was fixed for 24 hours in a 10% formalin solution (Sigma) and then transferred to 70% ethanol before paraffin embedded. Tissue was sectioned at a thickness of 5μm and was deparaffinized and rehydrated in an ethanol series. Sections were blocked with Background Sniper (Biocare Medical) for 15 minutes. H&E staining was performed according to common procedures (Sigma). Sections were stained with primary antibodies against synaptophysin (Invitrogen, 08-130, pre-diluted), SFRP1 (Abcam, ab4193, 1:1000), or NPR3 (Abcam, 37617, 1:100) overnight at 4 degrees. Sections were then incubated with secondary antibodies at 1:200 for 30 minutes at room temperature. Staining was developed by DAB (Vector Laboratories) followed by counterstaining with hematoxylin (Sigma) and mounted with Cytoseal (Thermo Scientific). For PD-1 staining, slides were subjected to a heat retrieval process at 120 degrees for 4 minutes before stained with anti-PD-1 antibody (R&D, AF1021, 0.8 μg/mL). Goat-on-Rodent HRP polymer (Biocare Medical) was used to detect anti-PD-1. For PD-L1 staining, a proprietary generated clone from Merck (MEB077.6H4.181) was used with a similar heat retrieval method. Rat-on-Mouse HRP

polymer (Biocare Medical) was used to detect anti-PD-L1. Microscopy was performed with Zeiss Axioplan 2 for IHC for subtype specific markers and Olympus IX70 for Ki-67 and caspase-3 IHC. Positive cell counts and marker density measurements were quantified using Image-Pro Premier 9. Images were generated using QImaging QCapture Pro 6 Software (QImaging Corporation) for the aforementioned IHC and an Aperio Scanscope slide scanner was used to generate images for IHC of PD-1 and PD-L1 staining.

Dissociation of tumor samples

To measure tumor-infiltrating immune cells in the Ptch1 MB and NSC MB tumors, symptomatic mice were sacrificed and tumors were removed. Tumors were dissociated to a single cell suspension following mechanical disruption and papain (Worthington) digestion. Cells were passed through a 70μm nylon mesh strainer (BD Biosciences) to remove large pieces and washed in PBS (Gibco). Cells were resuspended in a PBS solution with 2% fetal bovine serum (FBS) (Seradigm) and stained for 30 minutes at 4°C with respective antibodies or isotype controls. Samples were fixed in 1% formalin and run on a BD FACSCalibur.

Analysis of immune cell infiltrates

Dendritic cells were identified among dissociated tumor cells by co-expression of CD11c and I-A/I-E (MHC Class II). CD80 and CD40 were used as additional markers of activation on dendritic cells. CD3 expression was used to identify tumor-infiltrating lymphocytes and CD4 and CD8 were used to further distinguish the phenotype of the T cells. CTLA-4 and PD-1 expression were both measured as established markers of T cell suppression (14). Myeloid derived suppressor cells were identified by co expression CD11b and Gr-1 and tumor associated macrophages were distinguished by co-expression of CD11b and F4/80 (15). Rat anti-mouse IgG1 antibody was used to detect the PD-1 monoclonal antibody based on the mouse IgG1 isotype of the PD-1 blocking antibody. Antibody information is supplied in Supplemental Table 2. All samples were analyzed using FlowJo version 10 (Tree Star) and were gated on size and granularity, followed by omission of debris. For NSC MB samples, unstained NSC MB (GFP+) tumor cells were mixed with unstained Ptch1 MB (GFP−) tumor cells to set up voltage settings and used as a standard fluorescence minus one (FMO) control for samples stained in the FL-1 GFP and FL-2 PE channels. Therefore, false positives were avoided by excluding the FMO control, which comprised of intensely expressing GFP+ tumor cells. CaliBRITE 4 Color Beads (BD Biosciences) were used to determine compensation values. IgG controls were used to draw all gates. Total percentage values for infiltrating cells within NSC MB tumor samples were calculated by multiplying the non-GFP population by the percentage of positive cells determined within the non-GFP population. Calculations were confirmed by analysis of APC markers on the live cell gate of both tumor subtype populations, of which the emission spectra does not overlap with GFP in the FL-1 channel (Supplementary Figures 5-7). For display purposes, the number of events included on representative histogram plots of Ptch1 MB tumor infiltrates was increased to 2 $\times 10^4$ events. Comparative analyses were conducted using Prism (GraphPad).

Statistical analyses

Analysis of data comparing immune cell frequencies between MB subtypes was performed using the unpaired two-tailed t-test to assess means and standard deviations with a

significant result limited to p-values of less than 0.05. Survival curves were estimated for each group using the product-limit estimation of Kaplan and Meier. Primary comparative analysis of the curves for each group receiving various treatments was conducted using the log-rank test. All analyses were conducted using Prism (GraphPad).

Ex vivo expansion of T cells

Dendritic cells (DC) were isolated from the bone marrow of C57BL/6 mice using a previously published protocol with few modifications (16). Briefly, femurs and tibias of C57BL/6 mice were harvested and bone marrow flushed with RPMI (Gibco) + 10% FBS. Red cells were lysed and mononuclear cells were re-suspended in Complete DC Media (RPMI-1640, 5% heat-inactivated FBS, 1M HEPES, 55mM β-mercaptoethanol, 100mM sodium pyruvate, 10mM nonessential amino acids, 200mM L-glutamine, 10μg GM-CSF, 10μg IL-4, 5.5mL Penicillin/Streptomycin) and plated into 6-well plates at a density of 10^6 cells/mL. Non-adherent cells were discarded at day 3. At day 7, cells were re-plated onto 60mm tissue culture dishes. Resulting cells were electroporated the following day with 25μg of total RNA isolated from either Ptch1 MB or NSC MB. RNA-pulsed DCs were collected the following day and co-cultured with splenocytes for *ex vivo* expansion. Splenocytes harvested from tumor-bearing animals were expanded *ex vivo* using primary DCs pulsed with total tumor RNA and grown in T cell media (RPMI-1640, 10% heat-inactivated FBS, 55mM β-mercaptoethanol, 100mM sodium pyruvate, 10mM nonessential amino acids, 200mM L-glutamine, 5.5mL Penicillin/Streptomycin) and 100IU IL-2 for seven days before use in functional assays.

Functional stimulation assay

To determine anti-tumor T cell function, effector T cells were co-cultured with target cells overnight and supernatant was collected 48 hours later. A Cytometric Bead Array (CBA) kit was used to determine mouse Th1/Th2 cytokine release in the supernatant (BD Biosciences) as per manufacturer instructions.

Reagents and treatments

For immune checkpoint blockade experiments, anti-CTLA-4 and anti-PD-1 antibodies were first administered 5 days following intracranial tumor implantation. For CTLA-4 blockade, an initial dose of 100 μg anti-CTLA-4 (clone 9H10; BioXCell) was administered i.p., followed by three 50 μg maintenance doses every 3 days. For PD-1 blockade, mice were administered anti-PD-1 (mDX-400; Merck) i.p at a dose of 10mg/kg every 5 days for a total of 4 doses.

RESULTS

Generation and validation of immunocompetent animal models of SHH and Group 3 MB

We adapted two existing animal MB models recapitulating human SHH (Ptch1 MB) and Group 3 MB (NSC MB) tumors for immunotherapeutic preclinical evaluation. We stereotactically implanted tumors cells arising from the conventional *Ptch1+/−* model (17) and the MYC-driven model established by Pei et al. (13) into the cerebella of C57BL/6 mice (Supplementary Figure 1A). After six *in vivo* passages, we generated a large stock of

explanted tumor cells for subsequent preclinical studies. We observed that orthotopic transplantation of tumor cells from this frozen stock were not rejected by the host immune system. In order to determine a minimum tumorigenic dose required for uniform lethality within one month, animals were implanted with decreasing doses of tumor cells and measured for survival (Supplementary Figures 1B and 1C). We used the Affymetrix Mouse Genome 430 2.0 array to assess tumor mRNA expression for subtype-specific genes previously identified in the literature to ensure that *in vivo* passaging of both tumor lines in the C57BL/6 background did not change the identity of the tumor (18). We confirmed that both subtypes maintained expression of key subtype specific genes, including *Sfrp1* in the Ptch1 MB-tumor bearing animals (p=2.37×10^{-6}) and *Npr3* in NSC MB-tumor bearing animals (p=6.12×10^{-4}) (Supplementary Figure 2A and Supplementary Table 1). Immunohistochemistry for these markers also confirmed specific SFRP1 and NPR3 immunoreactivity. Both tumor subtypes were additionally stained with the neuronal marker synaptophysin, which was more diffusely expressed in the NSC MB subtype compared to the Ptch1 MB subtype. Transplanted Ptch1 MB tumors maintained histology associated with the original *Ptch1$^{+/-}$* model, displaying large areas of uniform cells with high nuclear to cytoplasmic ratio and round, hyperchromatic nuclei. Transplanted NSC MB tumors also conserved large cell anaplastic histology, consistent with the original MYC-amplified animal model of human Group 3 tumors (Supplementary Figure 2B). MB identification was also confirmed by a board-certified neuropathologist.

Characterization of immune cell infiltrates within tumor microenvironment

To analyze the endogenous infiltration of lymphocyte and myeloid cell populations, we measured proportions of immune cells from dissociated tumor tissue and compared them with normal cerebellar control samples (See Materials and Methods). We first evaluated the infiltration of antigen presenting cells (APCs) via co-expression of costimulatory molecules CD80 and CD40 and the expression of the MHC Class II molecule I-A/I-E on CD11c dendritic cells (DCs). Expression of CD80 on CD11c cells was not significantly different between the two MB subtypes (Figure 1A, p=0.1799); however, the Ptch1 MB subtype had significantly increased CD11c$^+$ CD40$^+$ (Figure 1B, p=0.04) and CD11c$^+$ I-A/I-E$^+$ (Figure 1C, p=0.03) cells.

Endogenous T-cell infiltration was determined using combined expression of CD3 and CD4 or CD8. Percentages of both infiltrating CD4 T cells (Figure 2A) and CD8 T cells (Figure 2B) were significantly higher within the Ptch1 MB tumor microenvironment compared to the NSC subtype (p=0.0034 and 0.0088, respectively). Both CD4 and CD8 T cell infiltration strongly correlated with DC infiltration into the Ptch1 MB tumor microenvironment (R^2 =0.9847 and 0.9986, respectively) (Supplementary Figure 3). No significant correlation between T cell infiltration and DC infiltration was observed in the NSC subtype, showing a negative trend (R^2 = 0.4048 and 0.1761 for CD4 and CD8, respectively) between the T cell subsets and DC infiltration (Supplementary Figure 4).

To assess the immunosuppressive state of tumor-infiltrating T cells, CTLA-4 expression on CD4 T cells and PD-1 expression on CD8 T cells were analyzed. No significant differences were observed for the CD4$^+$ CTLA-4$^+$ T cells between the two subtypes (Figure 2C,

p=0.64). Interestingly, there was a significantly higher proportion of CD8$^+$ PD-1$^+$ double positive T cells within the NSC MB microenvironment compared to Ptch1 MB (Figure 2D, p=0.004) suggesting a more profound immunologic suppression or exhaustion phenotype on T cells in these mice.

Due to significant differences observed in the proportions of suppressive CD8$^+$ PD-1$^+$ T cells, we evaluated levels of surface PD-L1 expression on both tumors. Overall PD-L1 expression in both tumor subtypes showed elevated expression compared to normal cerebellar controls, with the Ptch1 MB tumor expressing significantly more compared to the NSC MB tumor (Figure 3A, p=0.04). Because overall PD-L1 expression was relatively low in both subtypes compared to well-studied peripheral tumors such B16 melanoma (19), we hypothesized that the predominant source of PD-L1 originated from myeloid infiltrating cells. We evaluated the expression of PD-L1 on myeloid cells and observed significantly more CD11b$^+$ PD-L1$^+$ myeloid cells in the Ptch1 MB compared to NSC MB (Figure 3B, p=0.03). Myeloid cell infiltration was determined through the measurement of both myeloid derived suppressor cells (MDSCs) and tumor associated macrophages (TAMs). Combined expression of CD11b$^+$Gr-1$^+$ (MDSCs) or CD11b$^+$ F4/80$^+$ (TAMs) were also shown to be significantly higher in the Ptch1 MB tumor (Figures 3C and 3D, p= 0.01 and 0.03, respectively).

Differences in functional capacity of immune cells and response to immune checkpoint inhibitors

Because significant differences were observed in the infiltration of both CD4$^+$ and CD8$^+$ T cells and MDSCs and TAM cells, we hypothesized that the phenotypically undifferentiated nature of the NSC MB tumor contributed to a more immunologically "silent" profile compared to the more infiltrative Ptch1 MB tumor, and therefore lacked presentation of immunogenic antigens capable of eliciting reactivity from the immune system. To test the immunogenicity of antigens expressed by both MB subtypes, we harvested splenocytes from animals bearing intracranial NSC MB or Ptch1 MB and expanded them with primary dendritic cells electroporated with total tumor RNA from each subtype. The resulting effector T cells were tested for functionality and tumor specificity through a restimulation assay measuring specific TNFα and IFNγ release upon encounter with tumor target cells (Figure 4A). Despite differences in T cell and myeloid cell proportions, MB tumors expressed antigens capable of eliciting specific inflammatory immune responses. T cells generated from both the Ptch1 MB and NSC MB-tumor bearing animal showed significant Th1 cytokine release upon co-culture with tumor target cells compared to negative control cells pulsed with irrelevant antigen ovalbumin (OVA) RNA (Figures 4B and 4C).

While the antigenic profile of both MB subtypes did not differentially affect their immunogenic potential, we next assessed each subtype's response to immunotherapeutic intervention aimed on modulating the tumor microenvironment. Because the two subtypes contained significant differences in the CD8$^+$ PD-1$^+$ T cell population and no differences in the CD4$^+$ CTLA-4$^+$ T cell population, we used PD-1 and CTLA-4 blocking antibodies to determine if the differences in immunosuppressive T cell subsets could be leveraged to mediate antitumor efficacy *in vivo* (Figure 5A). Ptch1 MB tumor-bearing animals treated

with either anti-CTLA-4 alone, anti-PD-1 alone, or in combination, saw no treatment benefit over untreated tumor only controls (Figure 5B). However, in NSC MB tumor-bearing animals, animals treated with anti-PD-1 alone or in combination with anti-CTLA-4 showed a significant survival benefit over untreated controls (Figure 5C, p=0.02 and 0.009, respectively). Treatment in this model with anti-CTLA-4 alone showed no benefit, thus suggesting PD-1 expressing T cells as a key axis of immune suppression and tumor outgrowth in the NSC MB subtype, but not in the Ptch1 MB subtype.

To evaluate the effect of PD-1 blockade on both MB subtypes, we used IHC to assess expression of PD-1 and PD-L1 in untreated and anti-PD-1 treated tumors. IHC for PD-1 and PDL1 revealed PD-L1 reactivity to mainly arise from infiltrating cells and cells consistent with blood vessel endothelial cells. These findings corroborate our observations by flow cytometry, in that the predominant source of PD-L1 staining derived from non-tumor cell populations. In anti-PD-1 treated tumors, both subtypes demonstrated moderate increases in PD-1 and PD-L1 reactivity (Figure 5D). To determine the effect of PD-1 blockade on proliferation and apoptosis within MB tumors, we used IHC assess reactivity to Ki-67 and cleaved caspase-3. Both tumor subtypes exhibited a decrease in Ki-67 positive cells with the NSC MB subtype demonstrating a significant decrease (p=0.02). No significant changes were observed in caspase-3 reactivity between untreated and anti-PD-1 treated tumors in either MB subtype (Figure 5E).

PD-1 blockade occurs in the periphery and leads to increase in infiltrating lymphocytes

To elucidate whether the differential response to PD-1 blockade across MB subtypes was resultant of limitations in PD-1 antibody penetration of the blood brain barrier, we used flow cytometry to measure PD-1 monoclonal antibody (mAb) receptor occupancy following *in vivo* administration. As the PD-1 mAb is a mouse IgG1 isotype, we used a rat anti-mIgG1 antibody to detect the PD-1 mAb on infiltrating lymphocytes within the tumors, spleens, cervical lymph nodes (CLN) and inguinal lymph nodes (ILN) of both MB subtypes (Figure 6A). Significant PD-1 mAb was detected bound to the surface of T cells in the spleens, CLNs and ILNs of treated animals of both MB subtypes (Figure 6B). Of the PD-1 mAb detected in the spleen, CLN and ILN, the majority of antibody was bound to CD4 T cells compared to CD8 T cells (data not shown). Interestingly, there was no receptor occupancy (surface-bound anti-PD-1 antibody) observed within tumor infiltrating lymphocytes, demonstrating that anti-PD-1 antibodies were not detectable at appreciable levels in either tumor model. In contrast, systemic administration of anti-PD-1 antibodies led to a significant increase in the percentage of $CD3^+$ T cells within the tumor microenvironment of treated animals in both the Ptch1 and NSC MB tumors (Figure 6C, p=0.002 and 0.01, respectively). Further analysis of the infiltrating T cells revealed that these T cells represented a marked influx or expansion of PD-1 negative T cells within the tumor microenvironment (Figure 6D, p=0.01 for Ptch1 MB, p=0.02 for NSC MB). Similarly, evaluation of $CD8^+$ revealed significantly higher frequencies in treated animals of both MB subtypes (Figure 6E, p=0.004 for Ptch1 MB, p=0.01 for NSC MB). Evaluation of $CD4^+$ T cells in PD-1 treated animals revealed an increase in both MB subtypes, however, only the NSC MB subtype demonstrated a significant change in this compartment (Figure 6F, p=0.009). The results demonstrate that the efficacy of PD-1 blockade within the NSC MB model was not due to

differential accessibility of the tumor to monoclonal antibody penetration. In fact, tumor penetrance by the monoclonal antibody either directly or carried by infiltrating T cells is not observed within the context of efficacious immune checkpoint blockade.

DISCUSSION

Immunotherapy has gained significant credence as an effective strategy at redirecting the cytotoxic power of the immune system to target a multitude of malignancies (20⁻25). However, the examination of immune-based strategies in pediatric brain tumors has been marginal and requires a better understanding of the interplay between the immune system and the tumor microenvironment. This understanding promises to yield targeted immune-based therapies that can re-program distinct immune regulatory pathways across MB subgroups as well as enhance current antigen-targeted strategies.

Based on genetic profiling and immunohistochemical analyses of patient samples, a recent study by Margot et al. demonstrated a higher presence of tumor associated macrophages in the SHH-driven group of MB (8). Our study not only corroborates these findings, but is also the first to characterize immunologic differences within molecular subtypes of murine MB and demonstrate differential responses to immunotherapy in relevant preclinical models. These responses are likely secondary to the unique immune phenotypes among MB subgroups and our results suggest that strategies targeting the dominant immunologic phenotype within MBs and stratification of responses by molecular subtype should be considered.

We show that Ptch1 MB tumors contain higher percentages of infiltrating CD4$^+$ T cells and CD8$^+$ T cells. Interestingly, NSC MB tumors contain a higher proportion of CD8$^+$ PD-1$^+$ expression within the CD3$^+$ population. Differences in T cell proportions within the Ptch1 MB or NSC MB tumor microenvironment did not hinder the recognition of both subtypes by antigen-specific T cells and did not diminish Th1 cytokine responses *in vitro*. However, differential response to anti-PD-1 blockade in tumor-bearing animals suggests that the PD-1/PD-L1 axis is a key immunoregulatory pathway in Group 3 MBs that may unlock the potency of immunotherapeutic intervention. A previous study by Zeng et al. demonstrated the synergistic interaction of anti-PD-1 blockade in combination with stereotactic whole brain irradiation through the influx of CD8 T cells in treating intracranial malignant glioma (GL261) tumors (26), suggesting a CD8 requirement for abrogating tumor growth with a PD-1 blocking strategy. Depletion of the CD8 T cells resulted in the loss of efficacy while the depletion of CD4 T cells still yielded some benefit (26). In our experiments, the blockade of PD-1 pathway using anti-PD-1 monoclonal antibody as a monotherapy was sufficient to extend the median survival of treated animals in the NSC MB subtype but not SHH subtype despite clear evidence of a biologic response to PD-1 blockade and changes within the tumor microenvironment in both tumor models. It is possible that changes in the ratio of lymphocytes to other immunosuppressive cell populations within the tumor microenvironment may explain the refractory nature of SHH tumors in these experiments, as the greater baseline proportions of myeloid cells may require greater lymphocyte expansion to result in effective tumor rejections. Alternatively, the elevated PD-1 expression on

lymphocytes in the Group 3 model may be a marker more indicative of tumor where the PD-1/PD-L1 axis is a more relevant pathway for immune intervention.

Expression of PD-L1 on tumor cells has been demonstrated as an important prognostic indicator of response to anti-PD-1/PD-L1 therapy. In a Phase 1 trial testing anti-PD-1 in solid tumors, analyses of pre-treatment biopsies showed that the presence of membranous PD-L1 expression correlated to regressions in tumor growth following anti-PD-1 therapy (27). In our studies, we observed marginal surface PD-L1 expression on tumors of both MB tumor subtypes by both flow cytometry and IHC, of which was largely expressed by non-tumor cell populations, but differences in PD-L1$^+$ myeloid cells did not correlate with therapeutic benefit. Few studies have evaluated the prognostic value of PD-1 expressing tumor infiltrating lymphocyte (TIL) distribution at the tumor site (28). An examination of PD-1 expressing TILs in pre-treated solid tumor samples significantly correlated with PD-L1 expression on both tumor cells and immune cell infiltrates (29). In the same study, overall frequencies of TILs and PD-L1 expression on immune cell infiltrates did not significantly correlate to an objective clinical response to anti-PD-1 therapy; however, assessment of PD-1 expression on TILs was borderline associated with clinical response (29). Interestingly, our studies corroborate these observations and demonstrate that despite higher percentages of both myeloid and lymphocyte infiltration as well as increased frequencies of PD-L1 expressing myeloid infiltrating cells in Ptch1 MB tumor bearing animals, there was no response to PD-1 blockade in this subtype. PD-1 therapy did show efficacy in extending the median survival in NSC MB tumor bearing animals, suggesting that proportions of CD8+ PD-1+ expressing lymphocytes may serve as an indicator of response to PD-1 blockade and should be further evaluated in pre-treatment and post-treatment patient tumor samples.

We show that the Ptch1 MB tumor contains higher percentages of infiltrating MDSCs and TAMs, contributing to an increased immunologically suppressive tumor microenvironment. MDSCs and TAMs have long been characterized for their notable ability to negatively regulate innate and adaptive immune responses (15). The expansion and activation of myeloid infiltrating cells rely heavily on cytokines produced by tumor cells and activated T cells, directly leading to suppressive signaling pathways driven by the transcriptional factor STAT3 in MDSCs (30). Abad et al. observed similar increases in MDSC activity in spontaneously arising tumors in the Smo$^+$ transgenic mouse, a murine model of the SHH-driven MB. Conditional knockout of STAT3 in myeloid cells led to greater CD4 and CD8 infiltration with reduction in T regulatory cells and MDSCs (31). Despite higher proportions of lymphocyte subsets, our studies demonstrate that the Ptch1 MB model was less responsive to immune checkpoint inhibitors, and suggests that selective blockade of macrophage and myeloid derived suppressor populations may unlock intratumoral effector cells in SHH-driven MB (8). Additionally, as suggested by Margot et al., increased presence of myeloid and macrophage populations may be used to clinically stratify treatment and immunotherapeutic strategy. Examination of tumor-infiltrating lymphocyte to myeloid cell infiltrate ratios using proportions and absolute counts would be an interesting stratification between molecular subtypes and within responding versus non-responding tumors to perhaps provide further insights into the influences of tumor microenvironment on response to anti-PD-1 treatment.

Our detection of PD-1 mAb bound to the surface of T cells found only in the peripheral lymphoid organs, but not at the tumor site in anti-PD-1 treated animals suggests a systemic mechanism by which PD-1 blockade mediates antitumor efficacy within the brain. Our studies are the first to suggest that the physical presence of PD-1 antibody may not be required at the tumor site, specifically the brain, and potentially has important implications in PD-1 blocking strategies in other solid cancers. However, while no antibody was detected on the surface of tumor infiltrating T cells of sacrificed animals, we cannot rule out that the antibody may gain entry to the tumor site at different time points throughout tumor treatment than those examined in this study. Alternatively, T cells may rapidly internalize bound antibody, clearing it from the surface within the tumor microenvironment. We also acknowledge that PD-1 mAb binding to receptors on T cells within the tumor microenvironment could occur at levels below the limit of appreciable detection of our assay, thus necessitating further studies to confirm PD-1 receptor occupancy by PD-1 mAb within brain tumors. We observed however, significant influxes in PD-1 negative T cells in treated animals, with significant increases in the CD8 compartment. While treated animals of both tumor subtypes demonstrated increases in the CD4 infiltration, only the NSC MB subtype exhibited a significant increase. While this observation alone cannot explain why Ptch1 MB tumors are refractory to PD-1 blockade, the significant increase in CD4 may provide another clue as to why NSC MB responds to the PD-1 blockade. The mutational burden of a tumor has been demonstrated to be a predictor of response to PD-1/PD-L1 blocking strategies in non-small cell lung cancer (32, 33). In medulloblastoma, human Group 3 tumors have been characterized by amplifications of *MYC* and *OTX2* as well as alterations in numerous chromatin binding proteins. Such vast chromosomal aberrations and epigenetic changes, more numerous in the Group 3 compared to the SHH Group tumors, may contribute to the differential response observed by the two MB subtypes due to the presence of mutations and neoepitopes in the NSC MB tumor (34, 35). Recent findings have also identified predominant drivers of immune response to be linked to tumor specific mutations recognized by CD4^{+} cells (36). The influx of CD4^{+} cells observed in the NSC MB microenvironment following anti-PD-1 treatment may represent the antigen specific T cells responsible for driving the antitumor response.

In summary, this immunologic characterization of two MB animal models yields potential avenues to exploit functional intratumoral immune subsets that may induce antitumor immunity. Physiologic responses observed following PD-1 blockade despite the absence of PD-1 mAb within the tumor microenvironment demonstrate the efficacy of PD-1 blocking strategies in intracranial tumors by which the PD-1/PD-L1 axis is the main mechanism of immune suppression. Other strategies may be necessary in tumors such as the SHH MB subtype that exhibit alternative mechanisms of immune evasion. A better understanding of the immunological subtypes utilizing accurate patient molecular subtype classification will allow for novel targeted therapies stratified toward disease subsets, bypassing the morbid effects of current strategies.

Supplementary Material

Refer to Web version on PubMed Central for supplementary material.

References

1. Sirachainan N, Nuchprayoon I, Thanarattanakorn P, Pakakasama S, Lusawat A, Visudibhan A, et al. Outcome of medulloblastoma in children treated with reduced-dose radiation therapy plus adjuvant chemotherapy. J Clin Neurosci. 2011; 18(4):515–9. [PubMed: 21310618]

2. Packer RJ, Sposto R, Atkins TE, Sutton LN, Bruce DA, Siegel KR, et al. Quality of life in children with primitive neuroectodermal tumors (medulloblastoma) of the posterior fossa. Pediatr Neurosci. 1987; 13(4):169–75. [PubMed: 3454439]

3. Gururangan S, Krauser J, Watral MA, Driscoll T, Larrier N, Reardon DA, et al. Efficacy of high-dose chemotherapy or standard salvage therapy in patients with recurrent medulloblastoma. Neuro Oncol. 2008; 10(5):745–51. [PubMed: 18755919]

4. Northcott PA, Korshunov A, Pfister SM, Taylor MD. The clinical implications of medulloblastoma subgroups. Nature Reviews Neurology. 2012; 8:340–351. [PubMed: 22565209]

5. Mitchell DA, Sampson JH. Toward effective immunotherapy for the treatment of malignant brain tumors. Neurotherapeutics. 2009; 6(3):527–38. [PubMed: 19560742]

6. Okamoto Y, Shimizu K, Tamura K, Miyao Y, Yamada M, Matsui Y, et al. An adoptive immunotherapy of patients with medulloblastoma by lymphokine-activated killer cells (LAK). Acta Neurochir (Wien). 1988; 94(1-2):47–52. [PubMed: 3177046]

7. Caruso DA, Orme LM, Neale AM, Radcliff FJ, Amor GM, Maixner W, et al. Results of a phase 1 study utilizing monocyte-derived dendritic cells pulsed with tumor RNA in children and young adults with brain cancer. Neuro Oncol. 2004; 6(3):236–46. [PubMed: 15279716]

8. Margol A, Robison N, Gnanachandran J, Hung LT, Kennedy R, Vali M, et al. Tumor Associated Macrophages in SHH Subgroup of Medulloblastomas. Clin Cancer Res. 2014

9. Northcott PA, Korshunov A, Witt H, Hielscher T, Eberhart CG, Mack S, et al. Medulloblastoma comprises four distinct molecular variants. J Clin Oncol. 2011; 29(11):1408–14. [PubMed: 20823417]

10. Goodrich LV, Milenkovic L, Higgins KM, Scott MP. Altered neural cell fates and medulloblastoma in mouse patched mutants. Science. 1997; 277(5329):1109–13. [PubMed: 9262482]

11. Zurawel RH, Allen C, Wechsler-Reya R, Scott MP, Raffel C. Evidence that haploinsufficiency of Ptch leads to medulloblastoma in mice. Genes Chromosomes Cancer. 2000; 28(1):77–81. [PubMed: 10738305]

12. Wetmore C, Eberhart DE, Curran T. The normal patched allele is expressed in medulloblastomas from mice with heterozygous germ-line mutation of patched. Cancer Res. 2000; 60(8):2239–46. [PubMed: 10786690]

13. Pei Y, Moore CE, Wang J, Tewari AK, Eroshkin A, Cho YJ, et al. An animal model of MYC-driven medulloblastoma. Cancer Cell. 2012; 21(2):155–67. [PubMed: 22340590]

14. Wainwright DA, Chang AL, Dey M, Balyasnikova IV, Kim CK, Tobias A, et al. Durable therapeutic efficacy utilizing combinatorial blockade against IDO, CTLA-4, and PD-L1 in mice with brain tumors. Clin Cancer Res. 2014; 20(20):5290–301. [PubMed: 24691018]

15. Gabrilovich DI, Nagaraj S. Myeloid-derived suppressor cells as regulators of the immune system. Nat Rev Immunol. 2009; 9(3):162–74. [PubMed: 19197294]

16. Inaba K, Swiggard WJ, Steinman RM, Romani N, Schuler G, Brinster C. Isolation of dendritic cells. Curr Protoc Immunol. 2009 Chapter 3:Unit 3 7.

17. Yang ZJ, Ellis T, Markant SL, Read TA, Kessler JD, Bourboulas M, et al. Medulloblastoma can be initiated by deletion of Patched in lineage-restricted progenitors or stem cells. Cancer Cell. 2008; 14(2):135–45. [PubMed: 18691548]

18. Northcott PA, Korshunov A, Witt H, Hielscher T, Eberhart CG, Mack S, et al. Medulloblastoma Comprises Four Distinct Molecular Variants. Journal of Clinical Oncology. 2011; 29(11):1408–1414. [PubMed: 20823417]

19. Iwai Y, Ishida M, Tanaka Y, Okazaki T, Honjo T, Minato N. Involvement of PD-L1 on tumor cells in the escape from host immune system and tumor immunotherapy by PD-L1 blockade. Proc Natl Acad Sci U S A. 2002; 99(19):12293–7. [PubMed: 12218188]

20. Heiser A, Coleman D, Dannull J, Yancey D, Maurice MA, Lallas CD, et al. Autologous dendritic cells transfected with prostate-specific antigen RNA stimulate CTL responses against metastatic prostate tumors. J Clin Invest. 2002; 109(3):409–17. [PubMed: 11828001]

21. Kantoff PW, Higano CS, Shore ND, Berger ER, Small EJ, Penson DF, et al. Sipuleucel-T immunotherapy for castration-resistant prostate cancer. N Engl J Med. 2010; 363(5):411–22. [PubMed: 20818862]

22. Hodi FS, O'Day SJ, McDermott DF, Weber RW, Sosman JA, Haanen JB, et al. Improved survival with ipilimumab in patients with metastatic melanoma. N Engl J Med. 2010; 363(8):711–23. [PubMed: 20525992]

23. Topalian SL, Hodi FS, Brahmer JR, Gettinger SN, Smith DC, McDermott DF, et al. Safety, activity, and immune correlates of anti-PD-1 antibody in cancer. N Engl J Med. 2012; 366(26): 2443–54. [PubMed: 22658127]

24. Brahmer JR, Tykodi SS, Chow LQ, Hwu WJ, Topalian SL, Hwu P, et al. Safety and activity of anti-PD-L1 antibody in patients with advanced cancer. N Engl J Med. 2012; 366(26):2455–65. [PubMed: 22658128]

25. Schuster SJ, Neelapu SS, Gause BL, Janik JE, Muggia FM, Gockerman JP, et al. Vaccination with patient-specific tumor-derived antigen in first remission improves disease-free survival in follicular lymphoma. J Clin Oncol. 2011; 29(20):2787–94. [PubMed: 21632504]

26. Zeng J, See AP, Phallen J, Jackson CM, Belcaid Z, Ruzevick J, et al. Anti-PD-1 blockade and stereotactic radiation produce long-term survival in mice with intracranial gliomas. Int J Radiat Oncol Biol Phys. 2013; 86(2):343–9. [PubMed: 23462419]

27. Brahmer JR, Drake CG, Wollner I, Powderly JD, Picus J, Sharfman WH, et al. Phase I study of single-agent anti-programmed death-1 (MDX-1106) in refractory solid tumors: safety, clinical activity, pharmacodynamics, and immunologic correlates. J Clin Oncol. 2010; 28(19):3167–75. [PubMed: 20516446]

28. Tumeh PC, Harview CL, Yearley JH, Shintaku IP, Taylor EJ, Robert L, et al. PD-1 blockade induces responses by inhibiting adaptive immune resistance. Nature. 2014; 515(7528):568–71. [PubMed: 25428505]

29. Taube JM, Klein A, Brahmer JR, Xu H, Pan X, Kim JH, et al. Association of PD-1, PD-1 ligands, and other features of the tumor immune microenvironment with response to anti-PD-1 therapy. Clin Cancer Res. 2014; 20(19):5064–74. [PubMed: 24714771]

30. Gallina G, Dolcetti L, Serafini P, De Santo C, Marigo I, Colombo MP, et al. Tumors induce a subset of inflammatory monocytes with immunosuppressive activity on CD8+ T cells. J Clin Invest. 2006; 116(10):2777–90. [PubMed: 17016559]

31. Abad C, Nobuta H, Li J, Kasai A, Yong WH, Waschek JA. Targeted STAT3 disruption in myeloid cells alters immunosuppressor cell abundance in a murine model of spontaneous medulloblastoma. J Leukoc Biol. 2014; 95(2):357–67. [PubMed: 24068730]

32. Rizvi NA, Hellmann MD, Snyder A, Kvistborg P, Makarov V, Havel JJ, et al. Cancer immunology. Mutational landscape determines sensitivity to PD-1 blockade in non-small cell lung cancer. Science. 2015; 348(6230):124–8. [PubMed: 25765070]

33. Le DT, Uram JN, Wang H, Bartlett BR, Kemberling H, Eyring AD, et al. PD-1 Blockade in Tumors with Mismatch-Repair Deficiency. N Engl J Med. 2015; 372(26):2509–20. [PubMed: 26028255]

34. Northcott PA, Korshunov A, Pfister SM, Taylor MD. The clinical implications of medulloblastoma subgroups. Nat Rev Neurol. 2012; 8(6):340–51. [PubMed: 22565209]

35. Robinson G, Parker M, Kranenburg TA, Lu C, Chen X, Ding L, et al. Novel mutations target distinct subgroups of medulloblastoma. Nature. 2012; 488(7409):43–8. [PubMed: 22722829]

36. Kreiter S, Vormehr M, van de Roemer N, Diken M, Lower M, Diekmann J, et al. Mutant MHC class II epitopes drive therapeutic immune responses to cancer. Nature. 2015; 520(7549):692–6. [PubMed: 25901682]

TRANSLATIONAL RELEVANCE

Medulloblastoma remains incurable in one third of patients despite aggressive multi-modality standard therapies. The morbidities associated with such treatments make medulloblastoma an attractive candidate for immunotherapeutic intervention. However, little is known regarding the host immunologic interactions within the tumor microenvironment across molecular subtypes of medulloblastoma. Here, we demonstrate unique immune microenvironments and response to immune checkpoint blockade in syngeneic animal models of human SHH and Group 3 medulloblastomas. We analyzed immune cell infiltration in established intracranial tumors and report higher frequencies of myeloid cells and lymphocytes in SHH group tumors compared to Group 3 tumors. PD-1 expression was observed to be higher on lymphocytes within Group 3 medulloblastomas, and blockade of PD-1 conferred a significant antitumor effect in Group 3 tumors, but not in SHH tumors. Examination of receptor occupancy by anti-PD-1 monoclonal antibody demonstrated binding to T cells in the periphery but not to T cells within the tumor microenvironment. Systemic antibody treatment, however, resulted in a marked increase of PD-1 negative tumor-infiltrating lymphocytes after immune checkpoint blockade. Our work sheds light on the distinct immune profiles across molecular subtypes of medulloblastoma that may respond differentially to specific immunotherapeutic targeting strategies. These findings have relevant implications for the clinical development of immunotherapy targeting MB and potentially other cancers.

NSC MB **Ptch1 MB**

A **CD11c, CD80+ infiltration**

B **CD11c, CD40+ infiltration**

C **CD11c, I-A/I-E+ infiltration**
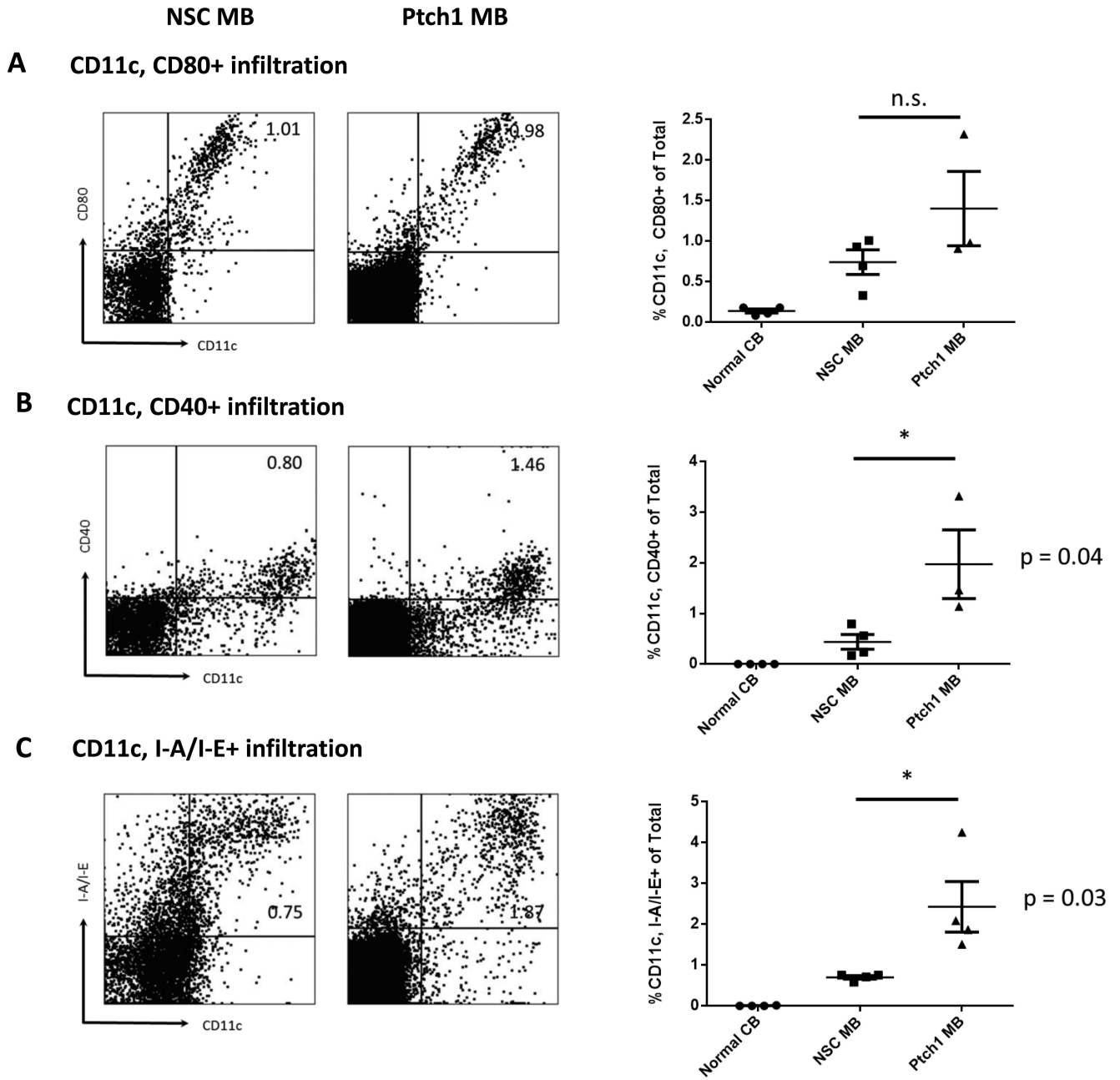
Figure 1. Characterization of markers of activation and antigen presentation in Ptch1 MB and NSC MB

Freshly dissociated tissue from moribund tumor-bearing animals and cerebella from normal animals was measured for markers of immune activation and antigen presentation by multi-color flow cytometry. Representative flow data with gating strategy are shown for each marker (left). Histograms of all samples for each tissue type are also shown (right). Percentages of CD11c+ cells costained with: (A) CD80, (B) CD40 and (C) I-A/I-E (MHC Class II). Percentages of CD11c, CD80+ were not significantly different between the two subtypes (p=0.17) but percentages of CD11c, CD40+ and CD11c, I-A/I-E+ cells were

significantly higher in the Ptch1 MB subtype compared to the NSC MB subtype (p=0.04 and 0.03 by unpaired t-test, respectively).
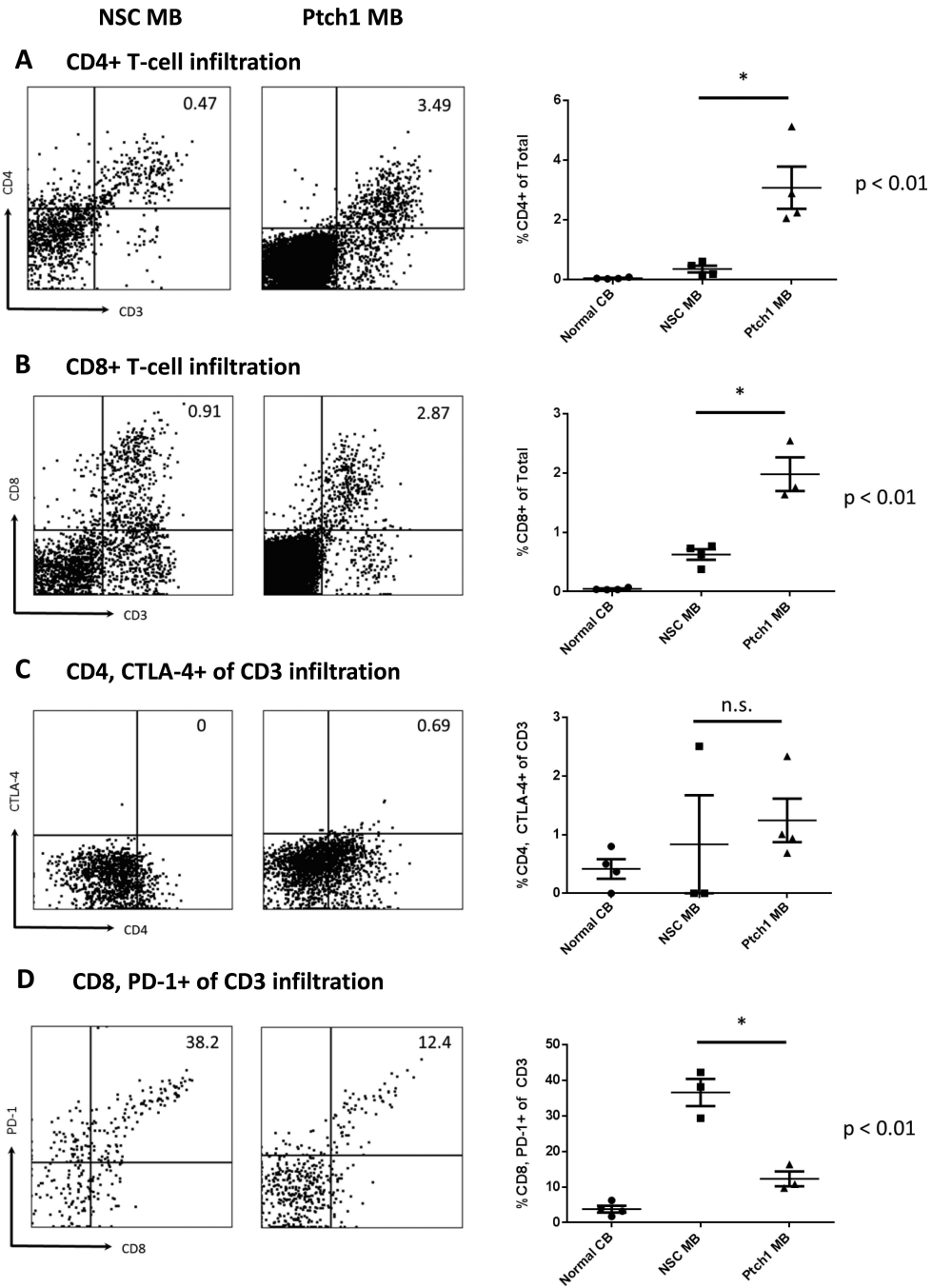
Figure 2. Characterization of infiltrating CD4 and CD8 T-cells in Ptch1 MB and NSC MB
T-cell infiltration in freshly dissociated tissue from moribund tumor-bearing animals and
cerebella from normal animals was measured by multi-color flow cytometry. Representative
flow data with gating strategy are shown for each marker (left). Histograms of all samples
for each tissue type are also shown (right). (A) Overall CD4+ and (B) CD8+ frequencies
were significantly higher in Ptch1 MB tumors (p=0.0088 and 0.0034 by unpaired t-test,
respectively). (C) Proportions of CD4+CTLA-4+ were not significantly different between

the two subtypes (p=0.64), but (D) CD8+PD-1+ of CD3 T cells was significantly higher in NSC MB tumor bearing animals (p=0.0049 by unpaired t-test).
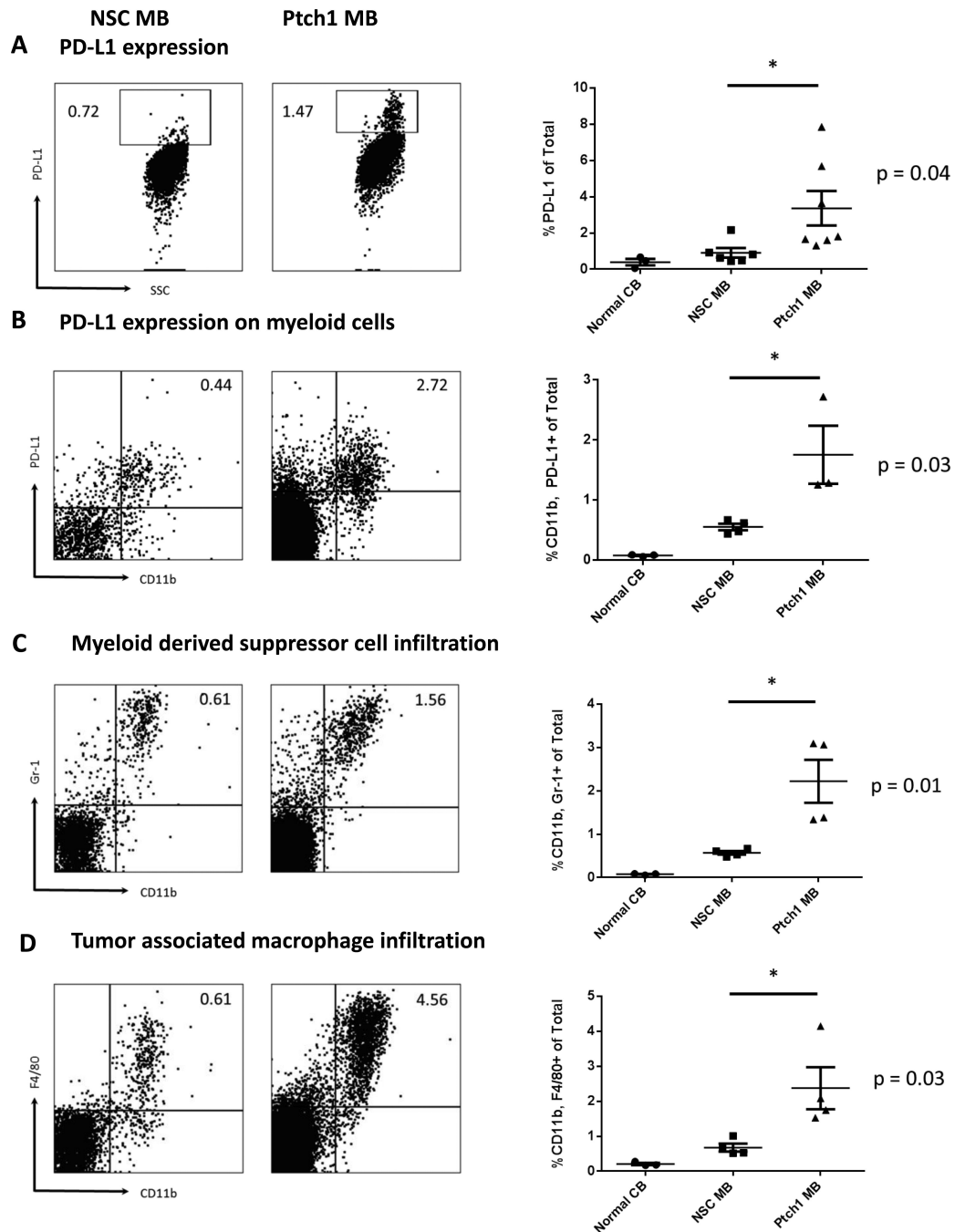
Figure 3. Evaluation of PD-L1 expression in Ptch1 MB and NSC MB

Freshly dissociated tumor from moribund tumor-bearing animals was stained for PD-L1 expression. Representative histograms NSC MB (left) and Ptch1 MB (right). (A) Percentage of PD-L1 expression on total cells was significantly higher in the Ptch1 MB subtype compared to the NSC MB subtype (p=0.04 by unpaired t-test). (B) PD-L1 co-expression on infiltrating myeloid cells was also significantly higher in the Ptch1 MB subtype (p=0.03 by unpaired t-test). (C) Myeloid derived suppressor cells and (D) tumor associated

macrophages infiltration frequencies were significantly higher in the Ptch1 MB subtype compared to the NSC MB subtype (p=0.01 and 0.03 by unpaired t-test, respectively).
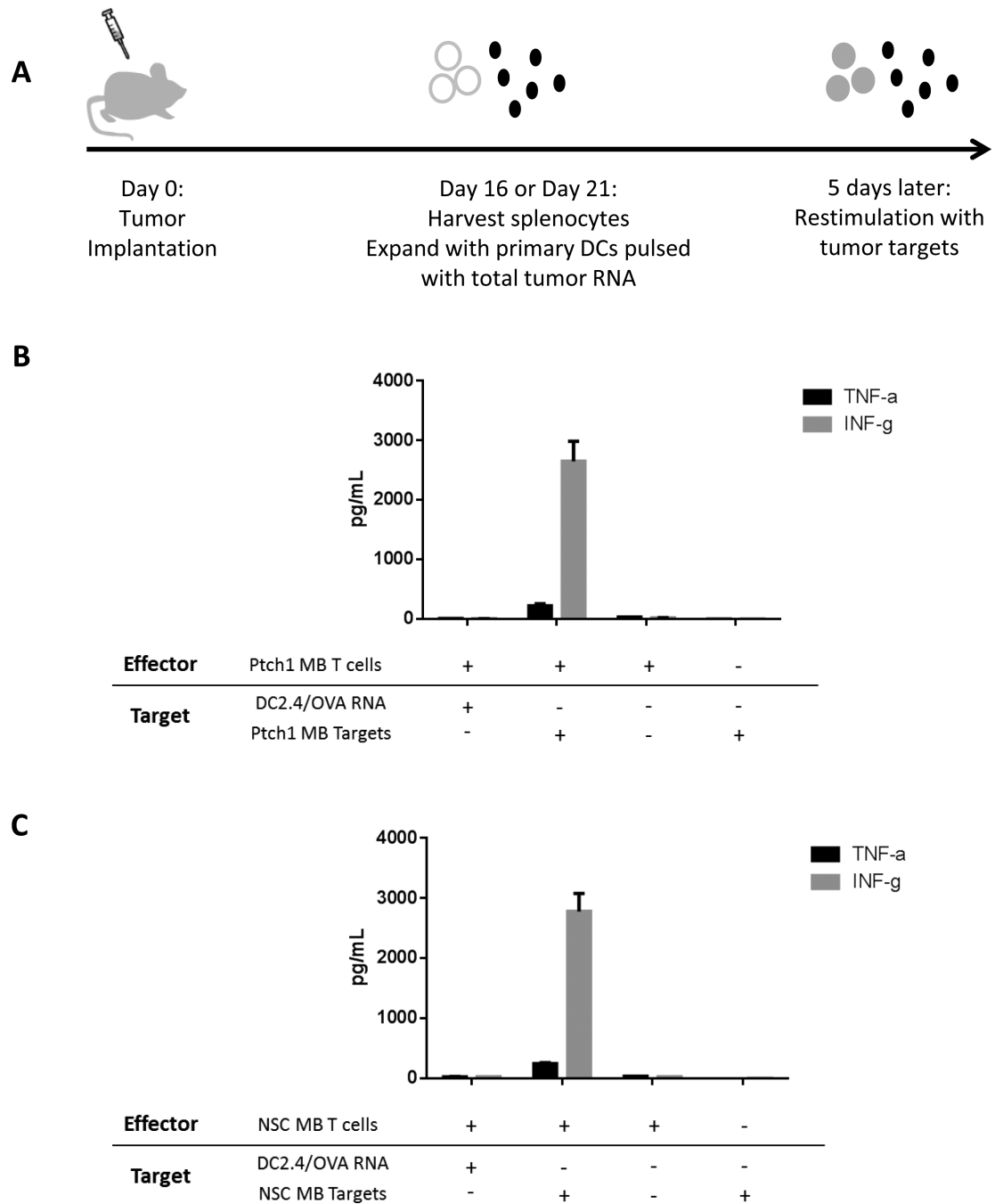
Figure 4. Immunologic differences within tumor microenvironment do not affect immunogenicity of total tumor antigens of both MB subtypes

Animals were implanted with the minimum tumorigenic dose of either NSC MB or Ptch1 MB tumor cells. (A) Splenocytes from tumor-bearing animals were harvested at Day 16 (NSC MB) or Day 21 (Ptch1 MB) and expanded with primary dendritic cells pulsed with total tumor RNA (ttRNA). (B) Splenocytes expanded with DCs pulsed with Ptch1 MB ttRNA or (C) NSC MB ttRNA showed specific Th1 responses upon restimulation with tumor targets.
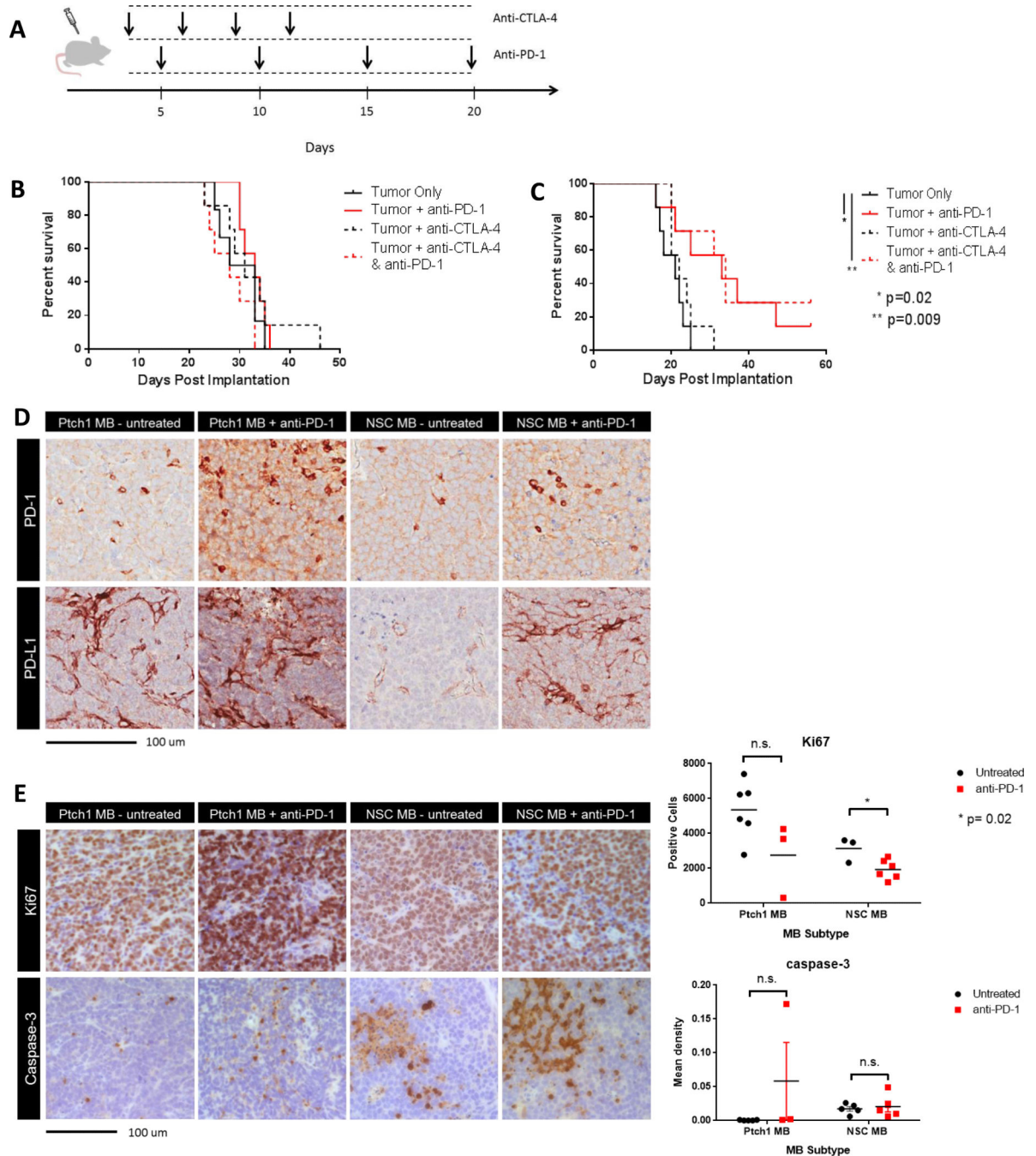
Figure 5. Anti-PD-1 blockade confers superior antitumor treatment effect in NSC MB tumor bearing animals

(A) Animals were implanted with the minimum tumorigenic dose of either NSC MB or Ptch1 MB tumor cells and administered CTLA-4 and PD-1 blocking antibodies, both alone and in combination. (B) Ptch1 MB tumor bearing animals did not respond to either CTLA-4 or PD-1 blockade whereas (C) NSC MB tumor bearing animals treated with anti-PD-1 alone and in combination with CTLA-4 blockade showed significant extension in median survival (p=0.02 and 0.009, respectively, by log-rank test, N=7 per group). (D) Explanted NSC MB and Ptch1 MB tumors from untreated and anti-PD-1 treated animals were stained for PD-1

and PD-L1 IHC. (E) Explanted NSC MB and Ptch1 MB tumors from untreated and anti-PD-1 treated animals were evaluated for differences in Ki67 and cleaved caspase-3 staining by IHC, with a significant decrease in Ki67 positive cells in anti-PD-1 treated NSC MB tumor bearing mice (top right, p=0.02 by unpaired t-test), but no significant differences in caspase-3 reactivity in both MB subtypes (bottom right).
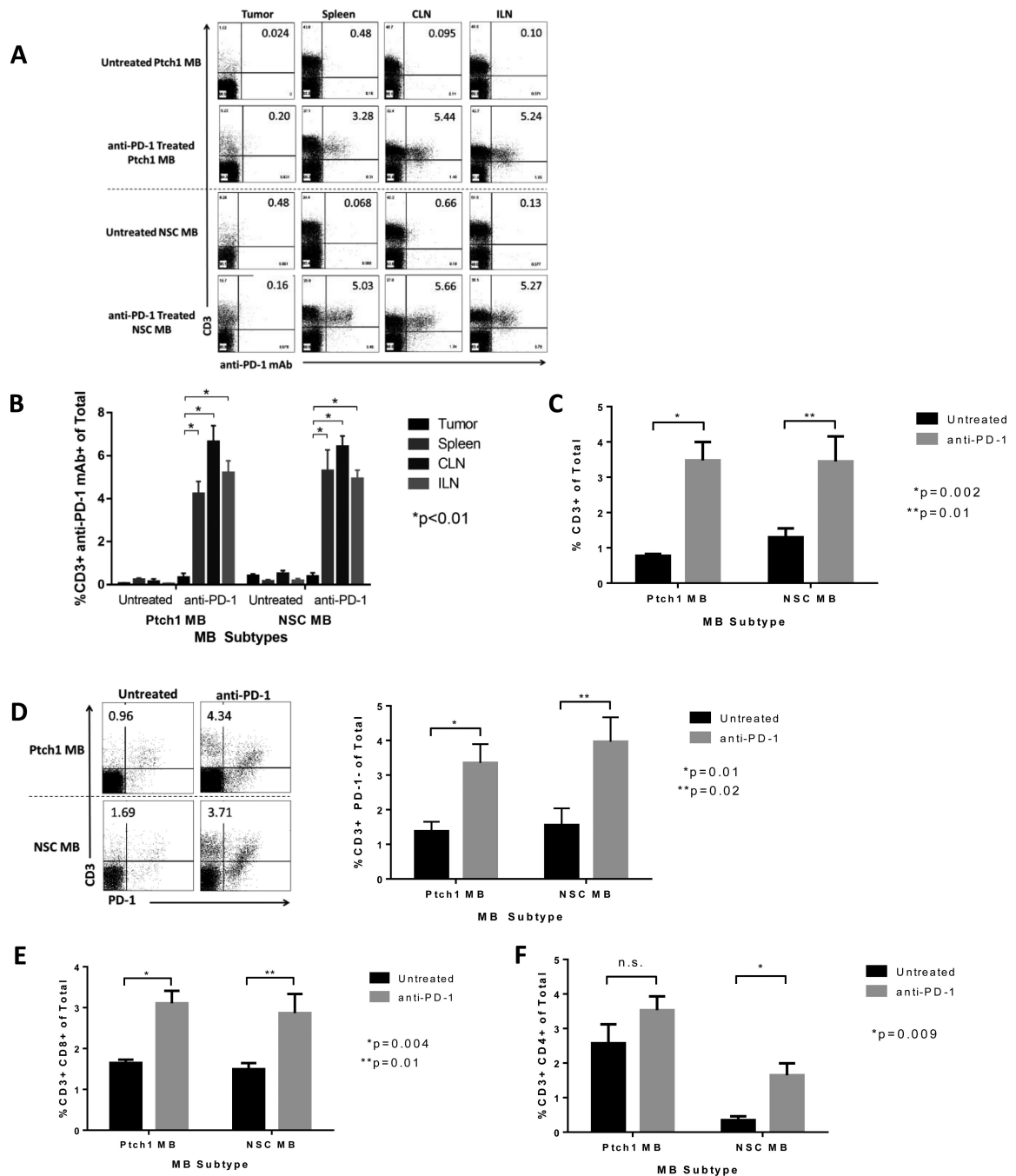
Figure 6. Anti-PD-1 blockade acts systemically and results in increased population of CD3 T cells within the tumor microenvironment

(A) Representative flow cytometric analyses of anti-PD-1 mAb staining via mIgG1 detection on CD3+ cells within the tumor, spleen, cervical lymph node (CLN) and inguinal lymph node (ILN). A rat anti-mouse IgG1 antibody was used to detect the anti-PD-1 mAb because it is a mouse IgG1 isotype. (B) Quantification of anti-PD-1 mAb positive CD3 T cells within the tumor and lymphoid organs of symptomatic tumor-bearing NSC and Ptch1 MB untreated controls and anti-PD-1 treated animals. (C) PD-1 blockade in both Ptch1 MB and NSC MB treated animals resulted in significant increases in CD3 infiltration (p=0.002 and 0.01 by

unpaired t-test, respectively). (D) Representative flow cytometric analyses (left) and histogram (right) of significantly increased CD3+ PD-1- infiltration in anti-PD-1 treated animals in both the Ptch1 and NSC MB subtypes (p=0.01 and 0.02 by unpaired t-test, respectively). (E) PD-1 blockade in both Ptch1 MB and NSC MB treated animals result in significant increases in CD8 infiltration (p=0.004 and 0.01 by unpaired t-test, respectively). (F) PD-1 blockade in both Ptch1 MB and NSC MB treated animals resulted in increases in CD4 infiltration, with a significant change in the NSC MB subtype (p=0.009 unpaired t-test).